

MoO₃ induces *p*-type Surface Conductivity by Surface Transfer Doping in Diamond

Kaijian Xing,¹ Yang Xiang,² Ming Jiang,² Daniel L. Creedon,³ Golrokh Akhgar,^{4, 5} Steve A. Yianni,¹ Haiyan Xiao, *,² Lothar Ley,⁶ Alastair Stacey,^{3, 7} Jeffrey C. McCallum,³ Serge Zhuiykov,⁸ Christopher I. Pakes *,¹ and Dong-Chen Qi *,^{1, 9}

¹ *Department of Chemistry and Physics, La Trobe Institute for Molecular Science, La Trobe University, Melbourne, Victoria 3086, Australia*

² *School of Physics, University of Electronic Science and Technology of China, Chengdu 610054, China*

³ *School of Physics, The University of Melbourne, Victoria 3010, Australia*

⁴ *ARC Centre of Excellence in Future Low-Energy Electronics Technologies, Monash University, Melbourne, Victoria 3800, Australia*

⁵ *School of Physics, RMIT University, Melbourne, Victoria 3001, Australia*

⁶ *Institute for Condensed Matter Physics, Universität Erlangen, Staudt-Str. 1, 91058 Erlangen, Germany*

⁷ *School of Science, RMIT University, Melbourne, Victoria 3001, Australia*

⁸ *Ghent University Global Campus, Department of Applied Analytical & Physical Chemistry, 119 Songdomunhwa-ro, Yeonsu-gu, Incheon, South Korea*

⁹ *School of Chemistry, Physics and Mechanical Engineering, Queensland University of Technology, Brisbane, Queensland 4001, Australia*

Abstract

Surface transfer doping of diamond using high electron affinity transition metal oxides (TMOs), such as MoO₃, has emerged as a key enabling technology for the development of diamond-based surface two-dimensional (2D) electronics. However, the omission of a critical

pre-annealing step in the device fabrication process to remove atmospheric adsorbates prior to TMO deposition, as seen in numerous studies, makes the role of TMOs ambiguous in light of air-induced surface conductivity, preventing a full understanding of the intrinsic surface transfer doping behavior of TMO-based surface acceptors. Here, using *in-situ* four-probe electrical measurements we explicitly show the insulating-to-conducting transition in diamond surface driven by MoO₃ induced surface transfer doping. Variable-temperature Hall-effect measurements reveal weak temperature-dependence down to 250 mK, evidencing the 2D Fermi liquid nature of the resulting surface conducting channel on diamond. Using first-principles calculations, we confirm the interfacial charge exchange upon MoO₃ adsorption leading to a degenerate hole conducting layer on diamond. This work provides significant insights into understanding the surface transfer doping of diamond induced by TMOs, and paves the way for the investigations of many interesting quantum transport properties in the resulting 2D hole conducting layer, such as phase-coherent magnetotransport, on diamond surface.

Keywords: diamond, molybdenum trioxide, 2DHG, surface conductivity, surface transfer doping

* Corresponding author. E-mail address: hyxiao@uestc.edu.cn; C.pakes@latrobe.edu.au; dongchen.qi@qut.edu.au

1. Introduction

Diamond has long been regarded as an ideal material for building high-power and high-frequency electronic devices because it is endowed with a range of outstanding electronic

properties among wide-bandgap semiconductors such as the highest breakdown voltage in excess of 10 MV/cm, exceptional intrinsic carrier mobility ($4500 \text{ cm}^2/\text{Vs}$ and $3800 \text{ cm}^2/\text{Vs}$ for electrons and holes, respectively), highest thermal conductivity ($22 \text{ Wcm}^{-1}\text{K}^{-1}$), and large carrier saturation velocity ($2.7 \times 10^7 \text{ cm/s}$ and $1.1 \times 10^7 \text{ cm/s}$ for electrons and holes, respectively) [1]. However, the development of diamond-based electronic devices has been severely impeded by a lack of effective bulk dopants for generation of charge carriers [2]. Although significant progresses have been made in the recent two decades in achieving *p*-type doping by boron and *n*-type doping by phosphorous or nitrogen [3], the inherently high ionisation energies (i.e. 0.36 eV for B, 0.57 eV for P, 1.7 eV for N) fundamentally limit the activation of the bulk dopants at room temperature, resulting in low charge carrier densities [2]. Following the observation of the air-induced surface conductivity (SC) of hydrogen-terminated diamond, an alternative doping scheme called surface transfer doping opens up new opportunities for diamond-based electronics by circumventing the challenges associated with conventional bulk doping. The surface transfer doping process relies on the spontaneous interfacial electron exchange between the valence band of diamond and the empty states of surface acceptors (e.g. solvated atmospheric molecules in the case of naturally-occurring, air induced SC), giving rise to a two dimensional (2D) hole accumulation layer on diamond [3, 4]. By exploiting this surface conducting layer on diamond, state of the art, high-performance metal-oxide-semiconductor field-effect transistors (MOSFETs) have been demonstrated with high drain current up to 1.3 A/mm [5], and a cut-off frequency up to 53 GHz [6].

Although high-performance diamond-based MOSFETs can be achieved by the surface transfer doping approach, the volatility of the atmospheric adsorbates results in instability of electronic device operation and limits the high-voltage operation [1]. In recent years, several groups have reported that using high-electron-affinity molecules, such as C_{60} [7], $\text{C}_{60}\text{F}_{48}$ [8],

F₄-TCNQ [9], as solid-state surface acceptors to replace the air-borne species could also induce the sub-surface *p*-type conductivity on hydrogen-terminated diamond. However, the poor thermal stability of these molecular acceptors has prevented this approach being used in a practical device architecture. More recently, high electron affinity transition metal oxides (TMOs), such as Nb₂O₅ [10], ReO₃ [11], WO₃ [10, 11], V₂O₅ [10, 12] and MoO₃ [10, 13~15], were reported as superior surface acceptors for diamond with enhanced thermal stability and induced hole density comparable to or higher than that induced by air. Based on the active conducting channel induced by TMO transfer doping, diamond-based MOSFETs have been demonstrated by Kalish *et al.* using either MoO₃ or WO₃ [16, 17] together with HfO₂ as the gate dielectric. Meanwhile, MoO₃ and V₂O₅ have also been incorporated as gate dielectrics in diamond MOSFETs by Hao *et al.* and Colangeli *et al.* [18~20]. However, the extent to which TMOs participate in the surface transfer doping process in these devices remains elusive because the air-induced SC was not intentionally removed in a high vacuum condition prior to the deposition of TMOs. Nevertheless, the promise that the TMO interfacial layer can serve simultaneously as surface acceptor, passivation layer and gate dielectric can significantly enhance the device design and process flexibility, enabling the development of high-performance and robust diamond electronics.

Despite mounting evidence showing that TMO could serve as a superior surface acceptor for hydrogen-terminated diamond, electrical characterization of the TMO-induced surface conducting channel on diamond reported in the literature was mostly done *ex-situ* (i.e. not in the same vacuum as the TMO deposition) and in some cases without a critical pre-annealing step that removes the atmospheric adsorbates prior to TMO deposition. Consequently, the possible confounding contribution from air-induced SC cannot be eliminated, preventing the formation of an understanding of the intrinsic surface transfer doping behavior of TMO-based

surface acceptors. The presence of residual atmospheric adsorbates at the diamond/TMO interface is also known to lead to degraded device performance over extended period of time [21]. Furthermore, an unusually strong spin-orbit coupling (SOC) in the air-induced surface conducting channel of diamond has been recently revealed by phase-coherent low-temperature magnetotransport measurements [22], and the SOC can be tuned over a wide range by ionic-liquid gating [23]. It would be of great interest to investigate the spin transport in the 2D hole gas (2DHG) induced by TMO doping, which would allow the study and development of all solid-state diamond spintronic devices. However, such a study typically requires cryogenic temperatures down to a few hundreds mK. Consequently, characterization of electrical transport in the TMO-induced surface conducting layer at low temperatures on diamond also becomes essential.

In this work, we demonstrate that MoO_3 serves as an excellent surface acceptor to yield the *p*-type conductivity on hydrogen-terminated diamond surface by a combination of electrical characterization and first-principles density functional theory (DFT) calculations. Using *in-situ* four-probe measurements, we show that the deposition of MoO_3 on a diamond surface, even at extremely low coverage, already yields a surface conductivity. Furthermore, the dependence of hole carrier density on MoO_3 coverage has been modelled successfully by the surface transfer doping model with a negative activation energy of the surface acceptors. Hall effect measurements in a temperature range from room temperature down to 250 mK further reveals the metallic conduction of the 2D hole layer induced by MoO_3 . The charge separation at the interface following MoO_3 adsorption and its impact on the electronic structures were also studied by DFT calculations.

2. Experimental Section

2.1 *In-situ four-probe measurement*

Commercial IIa (100) single crystal diamond samples (*Element Six*) were hydrogen-terminated in a microwave hydrogen plasma reactor (*ASTEX system*) operating at a power of 1700 W with a sample temperature of 850 °C for 10 minutes. *In-situ* characterization of the sheet resistance of a hydrogen-terminated diamond as a function of MoO₃ coverage was conducted using an in-vacuum four-point probe (*Jandel*) in a custom-built ultrahigh vacuum (UHV) system with a base pressure better than 5×10^{-10} mbar. The hydrogen-terminated diamond sample was firstly annealed at 400 °C for 30 minutes to completely desorb any surface adsorbates, reversing air-induced surface transfer doping. It should be noted that annealing in UHV condition at a temperature significantly below 800 °C will leave the hydrogen-termination intact, as evidenced by numerous reports [9, 12, 14, 24, 25]. After cooling the sample down to room temperature, MoO₃ was deposited on the diamond surface using a standard Knudsen cell operated at 475 °C with a deposition rate of ~ 0.125 Å/minute monitored by a quartz crystal microbalance (QCM). The nominal thickness of MoO₃ was calibrated using a correction factor independently determined by spectroscopic ellipsometry (J.A. Woollam M-2000DI). The sheet resistance of the diamond sample was then measured *in-situ* as a function of MoO₃ thickness with the four-point collinear probe by directly pressing the tips of the probe onto the sample surface, and the *I-V* characteristics was measured with a Keithley 2450 sourcemetre. The calculation of sheet resistance takes into consideration the geometrical corrections of both the sample dimension and the tip spacing [26].

2.2 *Hall bar device fabrication and MoO₃ deposition*

Hall bar devices (width 40 µm, length 200 µm) were fabricated on a hydrogen-terminated diamond following standard photolithography and lift-off processes. Device isolation was achieved by exposing the diamond surface to 50 W oxygen plasma at room temperature, while

keeping the active Hall-bar regions covered with a protective coating of photoresists and hence hydrogen terminated. The contact regions under electrodes consisted of a mixture of hydrogen- and oxygen-termination; this allowed electrical connection to the Hall-bar channel without compromising adhesion to contact metals. Ohmic contacts were formed by palladium (Pd) (100 nm) which shows significantly lower contact resistance than the commonly adopted Ti/Pt/Au contacts [27]. MoO₃ (20 nm) was then thermally deposited on the active Hall-bar channels through a shadow mask in an ultrahigh vacuum (UHV) system after the diamond sample was annealed up to 400 °C in the same vacuum for 30 minutes to desorb atmospheric adsorbates completely.

2.3 Hall effect measurements

Temperature-dependent Hall effect transport measurements of the diamond Hall-bar devices were performed in the temperature range from 250 mK to 20 K using a Leiden cryogenics dry dilution refrigerator with a 9-1-1 T superconducting vector magnet and between 77 K to 300 K in a Janis continuous flow liquid nitrogen cryostat equipped with a 0.7 T coil magnet, respectively. In the Janis system, a constant current of 1 μ A was supplied to the Hall-bar devices with a perpendicular sweeping magnetic field from - 0.7 T to + 0.7 T, whereas in the dilution refrigerator a constant current of 50 nA with a perpendicular sweeping magnetic field from - 2 T to + 2 T. The longitudinal voltage V_{xx} and the Hall voltage V_{xy} were then measured simultaneously to determine the corresponding resistivities ρ_{xx} and ρ_{xy} as a function of temperature. The much reduced current for measurements conducted in the dilution refrigerator were to reduce the effect of Joule heating on the temperature stability particular in sub-K regime. Standard low-frequency AC lock-in amplifiers (*Stanford Research Systems*) were employed in the Leiden Cryogenics dry refrigerator for achieving low-noise performance,

while standard DC measurements using a Keithley 2450 sourcemeter were employed in the Janis system.

2.4 Computational Details

All the density functional theory (DFT) calculations were performed using the Vienna *Ab Initio* Simulation Package (VASP) [28~30]. The interactions between ions and electrons were described by the projector augmented wave (PAW) pseudopotentials, and the exchange-correlation effects were treated using the generalized gradient approximation (GGA) in the Perdew-Burke-Ernzerhof (PBE) parameterization [31, 32]. The electronic configurations for the PAW potentials are $1s^1 2s^0 2p^0$ for H, $2s^2 p^2$ for C, $2s^2 2p^4$ for O and $5s^1 5p^0 4d^5$ for Mo. A repeated slab model was employed to simulate the hydrogen-terminated C (001) (2×1):H surface, which includes ten carbon atomic layers with 8 C atoms per layer and two hydrogen atomic layers with 8 H atoms per layer to saturate the dangling bonds. The slab was separated by a vacuum gap of 15 Å in the vertical direction. During the geometrical optimization, the MoO₃ molecule and the atoms in the top five layers were allowed to move freely, while the remaining atoms were fixed. The computations were based on a supercell consisting of 100 atoms with an 8×8×1 *k*-point sampling and a cut-off energy of 450 eV. The convergence criteria for total energies and forces were 10⁻⁴ eV and 10⁻⁴ eV/Å, respectively.

3. Results and Discussion

3.1 *In-situ* four-probe measurements

Figure 1a shows the sheet resistance of the diamond sample measured using the *in-situ* collinear four-point-probe as a function of MoO₃ thickness. The sample has an initial sheet resistance of 22.14 kΩ/□ measured in air and it slowly increased to 60.12 kΩ/□ after staying in vacuum for approximately 24 hours. After annealing in vacuum at 400 °C for 30 minutes, the

resistance measurement had exceeded the limit of the Keithley 2450 sourcemeter, suggesting that the surface conductivity had been sufficiently removed. The sheet resistance of the sample experienced a sharp reduction within the first few MoO₃ depositions: at a thickness of approximately 1.3 Å the sheet resistance of 9.95 kΩ/□ was already smaller than that of the initial air-doped value. The sheet resistance continued to drop with increasing MoO₃ thickness and began to saturate at around 5.8 kΩ/□ as a MoO₃ thickness of 6.5 Å was approached, corresponding approximately to 1 monolayer [33]. The sharp reduction of diamond sheet resistance at very low of MoO₃ coverage is consistent with photoemission measurements which reveal a significant upward band bending in diamond after the deposition of MoO₃ as low as 1 Å [14], confirming that MoO₃ acts as a highly efficient surface acceptor for surface transfer doping of diamond.

The hole density n_{2D} induced by MoO₃ doping has been extracted from the measured sheet resistance according to:

$$\rho_{xx} = \frac{1}{q \cdot \mu \cdot n_{2D}} \quad \text{Eq.(1)},$$

where q , μ , and ρ_{xx} are the elementary charge, carrier mobility, and sheet resistance, respectively. Since the carrier mobility in the hole conducting channel typically decreases with increasing hole density, assuming a constant hole mobility to extract the density values will result in an overestimation of the hole density at low MoO₃ coverages. With the absence of a theoretical relationship describing the dependence of mobility on hole density in the diamond surface conducting layer, in the Supplementary material (Figure S2a), we plotted the mobility as a function of $\log_{10}(n_{2D})$ based on an independent Hall effect dataset sampled from a large range of air-doped diamond samples, from which an empirical relationship

$\mu = A \times \log_{10}(n_{2D}) + B$, with A and B as fitting parameters, has been derived. Subsequently, Eq. (1) can be rewritten as:

$$\rho_{xx} = \frac{1}{q \cdot [A \cdot \log_{10}(n_{2D}) + B] \cdot n_{2D}} \quad \text{Eq.(2)},$$

which yields an empirical relationship between ρ_{xx} and n_{2D} as also plotted in Figure S2b.

Based on this empirical relationship, Figure 1b shows the variation of hole density as a function of MoO₃ coverage (solid circles). The hole density shows a similar dependence on the coverage to that of the sheet resistance as expected. It sees a sharp increase at low MoO₃ coverage and gradually saturates at high coverage reaching a final hole density of $2.8 \times 10^{13} \text{ cm}^{-2}$ at 1 monolayer thickness corresponding to MoO₃ coverage of $1.5 \times 10^{14} \text{ molecule/cm}^2$ coverage [33]. To corroborate the empirically determined hole density values, the same diamond sample after the last deposition of MoO₃ was then taken out of the UHV system and introduced into the Hall measurement system (Janis), and Hall effect measurements was performed in air on the sample in a Van de Pauw (VdP) configuration with silver paste contacts made to the four corners of the sample, yielding a hole density of $3 \times 10^{13} \text{ cm}^{-2}$ (open blue triangle in Figure 1b) which is in excellent agreement with that determined empirically above. It is also worth noting that MoO₃ induced SC on diamond appears to be stable after exposure to atmosphere, as the sheet resistance given by the Hall measurements barely changes (open blue triangle in Figure 1a) from the *in-vacuo* value.

The dependence of hole density induced by surface transfer doping on the coverage of surface acceptors can be modelled by considering Fermi-Dirac statistics and charge neutrality across the interface [7, 34]. The occupation of the MoO₃ molecular acceptor with one extra electron is given by the Fermi-Dirac probability:

$$n_{2D} = N_{A^*} = \frac{N_A}{\exp\left[\left(E_C^{\text{MoO}_3} - E_F\right)/kT\right] + 1} \quad \text{Eq.(3)},$$

in which N_A and N_{A^-} represent the total areal density of MoO_3 molecules and the negatively charged acceptors, respectively. k and T are the Boltzman constant and temperature, respectively. $E_C^{\text{MoO}_3}$ and E_F refer to the conduction band edge of MoO_3 , and the Fermi energy, respectively. The term $(E_C^{\text{MoO}_3} - E_F)$ in Eq. 3 can be related to the two energy terms Δ and u_s as:

$$E_C^{\text{MoO}_3} - E_F = (E_C^{\text{MoO}_3} - E_V^{\text{Diamond}}) + (E_V^{\text{Diamond}} - E_F) = \Delta + u_s(n_{2D}) \quad \text{Eq.(4)},$$

in which Δ is the acceptor energy, i.e. the energy difference between $E_C^{\text{MoO}_3}$ and E_V^{Diamond} (the valance band edge of diamond); $u_s(n_{2D})$, which is defined as the energy difference between the diamond valence band edge and the Fermi energy at the surface, is modulated by the upward band bending in diamond and it can be explicitly related to the areal hole density (Eq.S1 and Eq.S2 in the Supplementary material).

In the course of transfer doping, the charge transfer occurs across diamond- MoO_3 interface, and the spatial separation between electrons trapped in the MoO_3 layer and the holes confined to the diamond sub-surface accumulation layer induces an electric field, resulting in alteration of the energy band profile across the interface. The charge separation produces an interfacial dipole layer ($\Delta\Phi$) that lifts the vacuum level by the same amount together with the rest of the energy levels of the surface acceptors. The new acceptor energy can then be rewritten as $\Delta = \Delta_0 + \Delta\Phi$, in which Δ_0 represents the initial energy difference between $E_C^{\text{MoO}_3}$ and the E_V^{Diamond} . The interface dipole magnitude can be calculated as $\Delta\Phi(n_{2D}) = q^2 \cdot n_{2D} / C_{\square}$ according to a simple capacitor model. The specific capacitance of C_{\square} is determined as $1.4 \times 10^{13} \text{ e/cm}^2 \cdot \text{V}$ by assuming an effective permittivity of 1 and a separation distance of 0.75 nm [33]. Thus we can rewrite Eq. (4) as:

$$E_C^{\text{MoO}_3} - E_F = \Delta_0 + q^2 \cdot n_{2D} / C_{\square} + u_s(n_{2D}) \quad \text{Eq.(5)},$$

Eq. (5) represents the critical self-limiting mechanism in the surface transfer doping process. Both the interface dipole term and the band bending term experience an increase with increasing hole density. Collectively, they gradually lift the conduction band edge of MoO₃ relative to Fermi energy level of diamond and eventually stop at equilibrium. Substituting Eq. (5) into Eq. (3) further yields the relationship between n_{2D} and N_A :

$$n_{2D} = N_{A^-} = \frac{N_A}{\exp\left[\left(\Delta_0 + q^2 \cdot n_{2D} / C_{\square} + u_s(n_{2D})\right) / kT\right] + 1} \quad \text{Eq.(6)},$$

Eq. (6) allows one to quantitatively calculate the induced hole density in diamond for a given surface acceptor coverage N_A with a given initial activation energy Δ_0 .

In Fig.1 (b) we plot the theoretically derived carrier density as a function of MoO₃ coverage using Eq. 6 with Δ_0 as the only free parameter. The red solid line corresponding to the hole density calculated with an initial activation energy as $\Delta_0 = -2.3 \pm 0.1$ eV falls on the experimental data reasonably well. The deviation from experimental values at low coverage could be caused by uncertainties in the determination of the MoO₃ thickness. The obtained activation energy Δ_0 places the conduction band edge of MoO₃ 2.3 eV *below* the VBM of diamond when aligned by a common vacuum level. Then adopting the ionization potential of hydrogen-terminated diamond (IP = 4.2 eV) [35], the electron affinity of MoO₃ can be estimated as 6.5 ± 0.1 eV which is comparable with that in literature [14].

3.2 Variable temperature Hall effect measurements

The large negative activation energy of the MoO₃ surface acceptors, as discussed above, not only ensures a highly efficient surface transfer doping, but also implies that there won't be

carrier freeze-out in the resulting 2D hole conducting channel on diamond at low temperature since there is no thermal activation energy required to facilitate the interfacial electron exchange. Figure 2 shows temperature-dependent Hall effect measurements of the diamond hall-bar devices with MoO₃ transfer doping within a wide temperature range from 300 K down to 250 mK. Compared with the pristine air-doped device, the hole concentration shows an significant increase from $7.77 \times 10^{12} \text{ cm}^{-2}$ to $2.1 \times 10^{13} \text{ cm}^{-2}$ at 300 K after the deposition of 10 nm MoO₃ (Figure 2c), in good agreement with the value of $2.7 \times 10^{13} \text{ cm}^{-2}$ extracted from the *in-situ* four-point-probe measurement results. The increase in hole density leads to an overall reduction in the sheet resistance from $9.26 \text{ k}\Omega/\square$ to $5.39 \text{ k}\Omega/\square$ (Figure 2d). The MoO₃ doped Hall-bar device exhibits almost no temperature dependence both in terms of carrier density and sheet resistance in the temperature range from 20 K to 300 K, suggesting metallic rather than thermally activated conduction in the hole conducting channel induced by MoO₃ doping. Further cooling down to 250 mK, however, causes a moderate increase in sheet resistance from $6.3 \text{ k}\Omega/\square$ to $7.2 \text{ k}\Omega/\square$, corresponding to a decrease in carrier density from $2.17 \times 10^{13} \text{ cm}^{-2}$ to $1.57 \times 10^{13} \text{ cm}^{-2}$. This weak temperature dependence is logarithmic rather than exponential, as evidenced by the inset in Figure 2d which shows the sheet conductivity has a linear dependence with $\log_{10}(T)$ in the cryogenic temperature regime. A similar temperature dependence has been observed for both the air-induced and ionic-liquid gated surface conductivity in diamond [22, 23]. It is ascribed to the logarithmic quantum corrections, i.e. hole-hole interactions (HHI) and phase coherent quantum interference (in the form of weak localization and weak antilocalization), to the Drude conductivity in 2D systems at low temperature [20, 21, 36, 37]. Our results suggest a prevailing metallic conduction down to 250 mK supported by the surface transfer doping, manifesting the 2D Fermi liquid nature of this conducting channel.

3.3 DFT calculations

DFT calculations were carried out to gain a further understanding of the interaction between MoO₃ surface acceptors and the hydrogen-terminated diamond surface at atomic level. The energetically most preferable configuration for the adsorption of MoO₃ molecules on diamond surface was first explored by calculating the adsorption energy (ΔE) of MoO₃ on the hydrogen-terminated diamond surface for each configuration:

$$\Delta E = E_{\text{MoO}_3/\text{H-diamond}} - E_{\text{MoO}_3} - E_{\text{H-diamond}} \quad \text{Eq.(7)},$$

where $E_{\text{MoO}_3/\text{H-diamond}}$ and $E_{\text{H-diamond}}$ are the total energies of the relaxed hydrogen-terminated diamond surface with and without MoO₃, respectively, and E_{MoO_3} is the total energy of an isolated MoO₃ molecule [38]. In the present study, we considered 12 possible adsorptions configurations consisting of three initial adsorption orientations of MoO₃ molecules, namely parallel, titled and vertical (i.e. the normal direction of the triangular face defined by the three oxygen atoms of a MoO₃ tetrahedron is parallel, tilted and perpendicular, respectively, to the diamond surface), and within each orientation four adsorption sites are studied. The optimized structure for the 12 adsorptions configurations are presented in Figure S1 in the Supplementary material. The adsorption energy of -0.64 eV (here negative value indicates the adsorption nature) is the lowest for configuration P3 and V3, which have very similar adsorptions configurations with only slight differences in the atomic positions. These two configurations have notably longer vertical distance between Mo and the diamond surface, probably due to the repulsion between the positively charged Mo atoms and the hole-accumulating diamond surface. Meanwhile these configurations also maximise the potential O ... H—C interaction between the MoO₃ molecules and the hydrogen-terminated surface. Herein we have selected V3 to investigate the surface transfer doping between MoO₃ and hydrogen-terminated diamond surface in detail.

Figure 3a depicts the charge density difference $\Delta\rho$ between MoO₃ adsorbates and the hydrogen-terminated diamond surface. $\Delta\rho$ is defined as $\Delta\rho = \rho_{\text{MoO}_3/\text{H-diamond}} - \rho_{\text{MoO}_3} - \rho_{\text{H-diamond}}$, in where $\rho_{\text{MoO}_3/\text{H-diamond}}$ is the charge density of the hydrogen-terminated diamond surface with MoO₃ adsorption; ρ_{MoO_3} and $\rho_{\text{H-diamond}}$ are the charge densities of isolated MoO₃ molecules and the pristine hydrogen-terminated diamond surface, respectively [39]. Figure 3a illustrates the side-view and top-view of charge density differences for MoO₃-adsorbed diamond surface. The regions of electron accumulation and depletion are displayed in yellow and light blue, respectively. It is worth noting that there is a strong electron accumulation around O atoms of the MoO₃ molecules, while the electron depletion appears around the hydrogen-terminated surface of diamond. As a result, the adsorbed MoO₃ molecules and hydrogen-terminated diamond surface are negatively and positively charged, respectively. This demonstrates that electrons are transferred from the diamond surface to the MoO₃ adsorbates, leaving a hole accumulation layer as expected from the surface transfer doping model. The Bader charge population for the intrinsic and MoO₃ doped hydrogen-terminated diamond surface was performed to quantify the amount of hole density at the diamond surface. Each MoO₃ adsorbate extracts approximate 0.24 electrons from the top layer of the diamond surface, and the resulting areal hole density estimated from the amount of charge transferred per unit cell is determined to be $4.7 \times 10^{13} \text{ cm}^{-2}$ for a monolayer coverage of MoO₃; this is reasonably close to the hole density given by the four-probe and Hall effect measurements presented above. It is noted that the amount of electrons gained by each MoO₃ is generally comparable with other TMO-doped systems. Xiang et al. demonstrated that the CrO₃ dopant extracts approximate 0.36 electrons from the diamond surface, leaving a quasi 2D hole gas on the diamond surface [40]. Xia et al. also demonstrated that each MoO₃ molecule gains about 0.20 ~ 0.29 electrons from II-VI semiconductors (ZnS, CdS, ZnSe, CdSe) through

a similar surface transfer doping process [41]. The density of state (DOS) distribution of hydrogen-terminated diamond surface before and after MoO₃ adsorption is provided in Figure 3b to further explore the impact of interfacial charge transfer on electronic structures. As for MoO₃-doped hydrogen-terminated diamond surface, the Fermi level clearly moves into the top of diamond valence band indicative of strong *p*-type degenerate doping effect of MoO₃ and the metallic character of the doped diamond surface, which is consistent with the temperature-dependent transport measurements. On the other hand, the original acceptor state from MoO₃ becomes partially occupied by transferred electrons from the diamond valence band. The DFT results thus provide strong theoretical support for the interfacial charge transfer process and the excellent doping performance of MoO₃.

4. Conclusion

In summary, the intrinsic surface transfer doping behaviour of MoO₃ on diamond (001) has been studied by a combination of *in-situ* electrical characterization, variable-temperature Hall effect measurements and DFT calculations. We show that the very initial deposition of MoO₃ of 1.3 Å on a pre-annealed and hydrogen-terminated diamond surface already drastically reduces its sheet resistance, transforming it from highly insulating to conductive as a result of the surface transfer doping. The reduction of sheet resistance saturates around 1 monolayer coverage of MoO₃ with a final sheet resistance of 5.8 kΩ/□ corresponding to a hole density of $2.8 \times 10^{13} \text{ cm}^{-2}$ accumulated on the diamond. The surface transfer doping process can be fully described by the Fermi-Dirac statistics and charge neutrality considering a negative initial activation energy $\Delta_0 = -2.3 \pm 0.1 \text{ eV}$ dictated by the energy offset between the valence band edge of diamond and the conduction band edge of MoO₃. Low temperature transport measurements reveal a prevailing metallic conduction in the MoO₃ induced hole conducting channel down to 250 mK, manifesting its 2D Fermi liquid nature. The superior surface transfer

doping of MoO₃ is also corroborated by DFT calculations which confirms the charge exchange across the interface and the degenerate doping effect. Our study provides critical insights into the understanding of the surface transfer doping of diamond by high electron affinity TMOs, and has implication for the development of robust, integrated diamond surface electronic devices that harness the TMO-induced hole conducting channel. In particular, the metallic conducting channel at cryogenic temperature afforded by the surface transfer doping of MoO₃ paves the way for the investigations of many interesting quantum transport properties, such as phase-coherent magnetoresistance, in diamond surface.

Supplementary material

Supplementary material is available online or from the authors.

Acknowledgements

This work was supported by the Australian Research Council under the Discovery Project (No. DP150101673). Part of this work was performed at the Melbourne Centre for Nanofabrication (MCN) in the Victorian Node of the Australian National Fabrication Facility (ANFF). D. Q. acknowledges the support of the Australian Research Council (Grant No. FT60100207). A. S. acknowledges the Australian Research Council through Grant No. DE170100129, LP160101515. We also thank A. Tadich of the Australian Synchrotron for technical help with MoO₃ deposition on Hall bar devices and in-air four-point-probe sheet resistance measurements.

Founding source

The Australian Research Council (Grant No. FT60100207) (Grant No. DP150101673) (Grant No. DE170100129) (Grant No. LP160101515)

Declaration of interests

The authors declare that they have no known competing financial interests or personal relationships that could have appeared to influence the work reported in this paper.

References

- [1] Kasu, M.; Ueda, K.; Yamauchi, Y.; Tallaire, A.; Makimoto, T., Diamond-Based RF Power Transistors: Fundamentals and Applications, *Diam. Relat. Mater.* 16 (2007), 1010–1015.
- [2] Geis, M. W.; Wade, T. C.; Wuorio, C. H.; Fedynyshyn, T. H.; Duncan, B.; Plaut, M. E.; Varghese, J. O.; Warnock, S. M.; Vitale, S. A.; Hollis, M. A. Progress Toward Diamond Power Field-Effect Transistors. *Phys. Status Solidi Appl. Mater. Sci.* 215 (2018), 1800681.
- [3] Pakes, C. I.; Garrido, J. a.; Kawarada, H., Diamond Surface Conductivity: Properties, Devices, and Sensors, *MRS Bull.* 39 (2014), 542–548.
- [4] Maier, F.; Riedel, M.; Mantel, B.; Ristein, J.; Ley, L., Origin of Surface Conductivity in Diamond, *Phys. Rev. Lett.* 85 (2000), 3472–3475.
- [5] Hirama, K.; Sato, H.; Harada, Y.; Yamamoto, H.; Kasu, M., Diamond Field-Effect Transistors with 1.3 A/mm Drain Current Density by Al₂O₃ Passivation Layer, *Jpn. J. Appl. Phys.* 51 (2012), 090112.
- [6] Russell, S.; Sharabi, S.; Tallaire, A.; Moran, D. A. J., RF Operation of Hydrogen-Terminated Diamond Field Effect Transistors: A Comparative Study, *IEEE Trans. Electron Devices* 62 (2015), 751–756.
- [7] Strobel, P.; Riedel, M.; Ristein, J.; Ley, L., Surface Transfer Doping of Diamond, *Nature*

- 430 (2004), 439–441.
- [8] Edmonds, M. T.; Wanke, M.; Tadich, A.; Vulling, H. M.; Rietwyk, K. J.; Sharp, P. L.; Stark, C. B.; Smets, Y.; Schenk, A.; Wu, Q. H., Surface Transfer Doping of Hydrogen-Terminated Diamond by C₆₀F₄₈: Energy Level Scheme and Doping Efficiency, *J. Chem. Phys.* 136 (2012), 124701.
 - [9] Qi, D.; Chen, W.; Gao, X.; Wang, L.; Chen, S.; Loh, K. P.; Wee, A. T. S., Surface Transfer Doping of Diamond (001) by Tetrafluoro-Tetracyanoquinodimethane, *J. Am. Chem. Soc.* 129 (2007), 8084–8085.
 - [10] Verona, C.; Ciccognani, W.; Colangeli, S.; Limiti, E.; Marinelli, M.; Verona-Rinati, G., Comparative Investigation of Surface Transfer Doping of Hydrogen Terminated Diamond by High Electron Affinity Insulators, *J. Appl. Phys.* 120 (2016), 025104.
 - [11] Tordjman, M.; Weinfeld, K.; Kalish, R., Boosting Surface Charge-Transfer Doping Efficiency and Robustness of Diamond with WO₃ and ReO₃, *Appl. Phys. Lett.* 111 (2017), 111601.
 - [12] Crawford, K. G.; Cao, L.; Qi, D.; Tallaire, A.; Limiti, E.; Verona, C.; Wee, A. T. S.; Moran, D. A. J., Enhanced Surface Transfer Doping of Diamond by V₂O₅ with Improved Thermal Stability, *Appl. Phys. Lett.* 108 (2016), 2–6.
 - [13] Yin, Z.; Tordjman, M.; Lee, Y.; Vardi, A.; Kalish, R.; Del Alamo, J. A., Enhanced Transport in Transistor by Tuning Transition-Metal Oxide Electronic States Interfaced with Diamond, *Sci. Adv.* 4 (2018), eaau0480.
 - [14] Russell, S. A. O.; Cao, L.; Qi, D.; Tallaire, A.; Crawford, K. G.; Wee, A. T. S.; Moran, D. A. J., Surface Transfer Doping of Diamond by MoO₃: A Combined Spectroscopic and Hall Measurement Study, *Appl. Phys. Lett.* 103 (2013), 3–7.
 - [15] Tordjman, M.; Saguy, C.; Bolker, A.; Kalish, R., Superior Surface Transfer Doping of Diamond with MoO₃, *Adv. Mater. Interfaces* 1 (2014), 1300155.

- [16] Vardi, A.; Tordjman, M.; Del Alamo, J. A.; Kalish, R., A Diamond:H/MoO₃ MOSFET, IEEE Electron Device Lett. 35 (2014), 1320–1322.
- [17] Yin, Z.; Tordjman, M.; Vardi, A.; Kalish, R.; Alamo, J. A.; Diamond, A. A.; Wo, H., A Diamond : H/WO₃ Metal–Oxide–Semiconductor Field-Effect Transistor, IEEE Electron Device Lett. 39 (2018), 540–543.
- [18] Ren, Z.; Zhang, J.; Zhang, J.; Zhang, C.; Xu, S.; Li, Y.; Hao, Y., Diamond Field Effect Transistors With MoO₃ Gate Dielectric, IEEE Electron Device Lett. 38 (2017), 786–789.
- [19] Ren, Z.; Zhang, J.; Zhang, J.; Zhang, C.; Chen, D.; Yang, P.; Li, Y.; Hao, Y., Polycrystalline Diamond MOSFET With MoO₃ Gate Dielectric and Passivation Layer, IEEE Electron Device Lett. 38 (2017), 1302–1304.
- [20] Colangeli, S.; Verona, C.; Ciccognani, W.; Marinelli, M.; Rinati, G Verona.; Limiti, E.; Benetti, M.; Cannata, D.; Di Pietrantonio, F., H-Terminated Diamond MISFETs with V₂O₅ as Insulator, 2016 IEEE Compound Semiconductor Integrated Circuit Symposium (CSICS) . 2016, 1–4.
- [21] Crawford, K. G.; Qi, D.; McGlynn, J.; Ivanov, T. G.; Shah, P. B.; Weil, J.; Tallaire, A.; Ganin, A. Y.; Moran, D. A. J., Thermally Stable, High Performance Transfer Doping of Diamond Using Transition Metal Oxides, Sci. Rep. 8 (2018), 1–9.
- [22] Edmonds, M. T.; Willems Van Beveren, L. H.; Klochan, O.; Cervenka, J.; Ganesan, K.; Prawer, S.; Ley, L.; Hamilton, A. R.; Pakes, C. I., Spin-Orbit Interaction in a Two-Dimensional Hole Gas at the Surface of Hydrogenated Diamond, Nano Lett. 15 (2015), 16–20.
- [23] Akhgar, G.; Klochan, O.; Willems Van Beveren, L. H.; Edmonds, M. T.; Maier, F.; Spencer, B. J.; McCallum, J. C.; Ley, L.; Hamilton, A. R.; Pakes, C. I., Strong and Tunable Spin-Orbit Coupling in a Two-Dimensional Hole Gas in Ionic-Liquid Gated Diamond Devices, Nano Lett. 16 (2016), 3768–3773.

- [24] Riedel, M.; Ristein, J.; Ley, L. Recovery of Surface Conductivity of H-Terminated Diamond after Thermal Annealing in Vacuum. *Phys. Rev.* 69 (2004), 125338.
- [25] Graupner, R.; Maier, F.; Ristein, J.; Ley, L.; and Jung, C. High-resolution surface-sensitive C 1s core-level spectra of clean and hydrogen-terminated diamond (100) and (111) surfaces, *Phys. Rev. B* 57(1998), 12397.
- [26] Smits, F. M., Measurement of Sheet Resistivities with the Four-Point Probe, *Bell Syst. Tech. Pap.* 37 (1957), 711–718.
- [27] Wang, W.; Hu, C.; Li, F. N.; Li, S. Y.; Liu, Z. C.; Wang, F.; Fu, J.; Wang, H. X., Palladium Ohmic Contact on Hydrogen-Terminated Single Crystal Diamond Film, *Diam. Relat. Mater.* 59 (2015), 90–94.
- [28] Kresse, G.; Furthmuller, J., Efficient Iterative Schemes for Ab Initio Total Energy Calculations Using a Plane-Wave Basis Set, *Phys. Rev. B* 54 (1996), 11169–11186.
- [29] Kresse, G.; Furthmüller, J., Efficiency of Ab Initio Total Energy Calculations for Metals and Semiconductors Using a Plane Wave Basis Set, *Comput. Mat. Sci.* 6 (1996), 15–50.
- [30] Kresse, G.; Joubert, D., From Ultrasoft Pseudopotentials to the Projector Augmented - Wave Method, *Phys. Rev. B* 59 (1999), 1758–1775.
- [31] Perdew., J. P.; Burken, K.; Ernzerhof, M., Generalized Gradient Approximation Made Simple, *Phys. Rev. Lett.* 77 (1996), 3865–3868.
- [32] P.E.Bloch., Projector Augmented-Wave Method, *Phys. RE* 50 (1994), 17953–17979.
- [33] Kalantar-Zadeh, K.; Tang, J.; Wang, M.; Wang, K. L.; Shailos, A.; Galatsis, K.; Kojima, R.; Strong, V.; Lech, A.; Wlodarski, W., Synthesis of Nanometre-Thick MoO₃ Sheets, *Nanoscale* 2 (2010), 429–433.
- [34] Strobel, P.; Riedel, M.; Ristein, J.; Ley, L.; Boltalina, O., Surface Transfer Doping of Diamond by Fullerene, *Diam. Relat. Mater.* 14 (2005), 451–458.
- [35] Ley, L. Surface Conductivity of Diamond. In *CVD Diamond for Electronic Devices and*

- Sensors, Ricardo S. Sussmann; John Wiley & Sons Ltd. United Kingdom, 2009, 69–102.
- [36] Al'tshuler, B. L.; Aronov, A. G.; Larkin, A. I.; Khmel'nitskii, D. E., The Anomalous Magnetoresistance in Semiconductors, *Sov. Phys. JETP* 54 (1981), 411–419.
 - [37] P.D. Dresselhaus, C.M.A.Papavassiliou, R. G. W., Observation of Spin Precession in GaAs Inversion Layer Using Antilocalization, *Phys. Rev. Lett.* 68 (1992), 106–109.
 - [38] Beheshtian, J.; Peyghan, A. A.; Bagheri, Z., Detection of Phosgene by Sc-Doped BN Nanotubes: A DFT Study, *Sensors Actuators, B Chem.* 171 (2012), 846–852.
 - [39] Young, H. X.; Yu, Y.; Xu, L. F.; Gu, C. Z., Ab Initio Study of Molecular Adsorption on Hydrogenated Diamond (001) Surfaces, *J. Phys. Conf. Ser.* 29 (2006), 145–149.
 - [40] Xiang, Y.; Jiang, M.; Xiao, H.; Xing, K.; Peng, X.; Zhang, S., Applied Surface Science A DFT Study of the Surface Charge Transfer Doping of Diamond by Chromium Trioxide, *Appl. Surf. Sci.* 496 (2019), 143604.
 - [41] Xia, F.; Shao, Z.; He, Y.; Wang, R.; Wu, X.; Jiang, T.; Duhm, S.; Zhao, J.; Lee, S. T.; Jie, J., Surface Charge Transfer Doping via Transition Metal Oxides for Efficient P-Type Doping of II-VI Nanostructures, *ACS Nano* 10 (2016), 10283–10293.

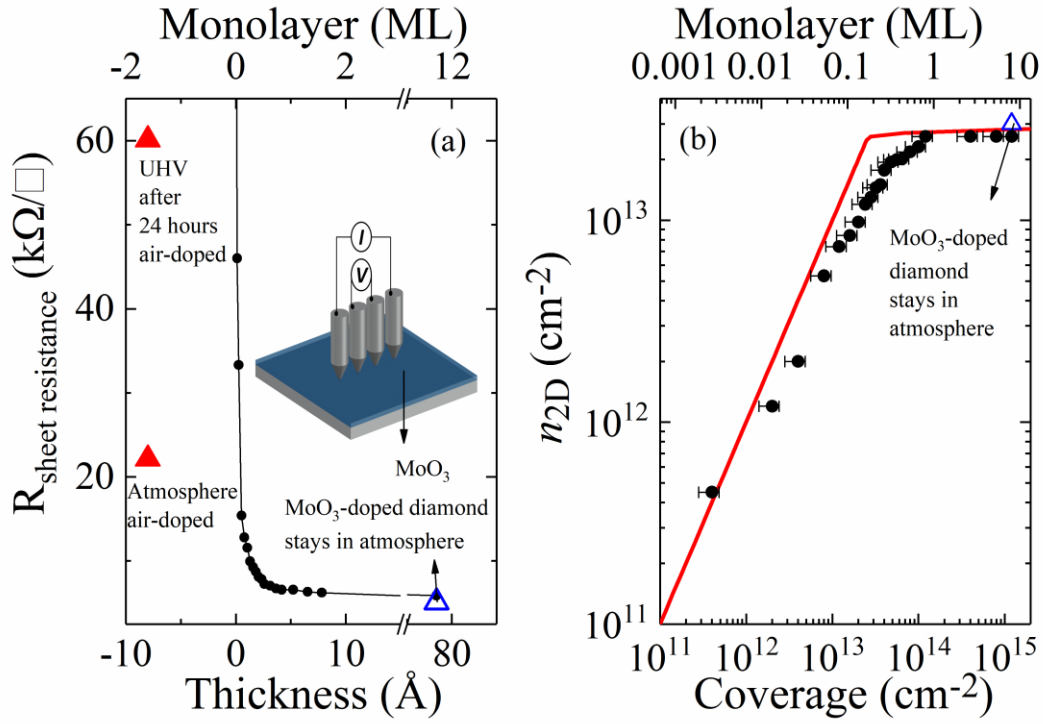


Figure 1. (a) Sheet resistance of diamond with increasing MoO₃ coverage. The solid red triangles represent the sheet resistance of air-doped hydrogen-terminated diamond measured in both atmosphere and UHV condition. The open blue triangle represents the sheet resistance of MoO₃ doped hydrogen-terminated diamond measured in atmosphere. (b) Experimentally and theoretically determined carrier concentration as a function of MoO₃ coverage. The black solid circles represent the experimental data. The red solid line corresponds to the theoretical data calculated using Eq. (6) with the initial activation energy (Δ_0) of $-(2.3 \pm 0.1)$ eV. The open blue triangle represents the hole density of MoO₃ doped hydrogen-terminated diamond measured in atmosphere by Hall effect measurements in VdP geometry

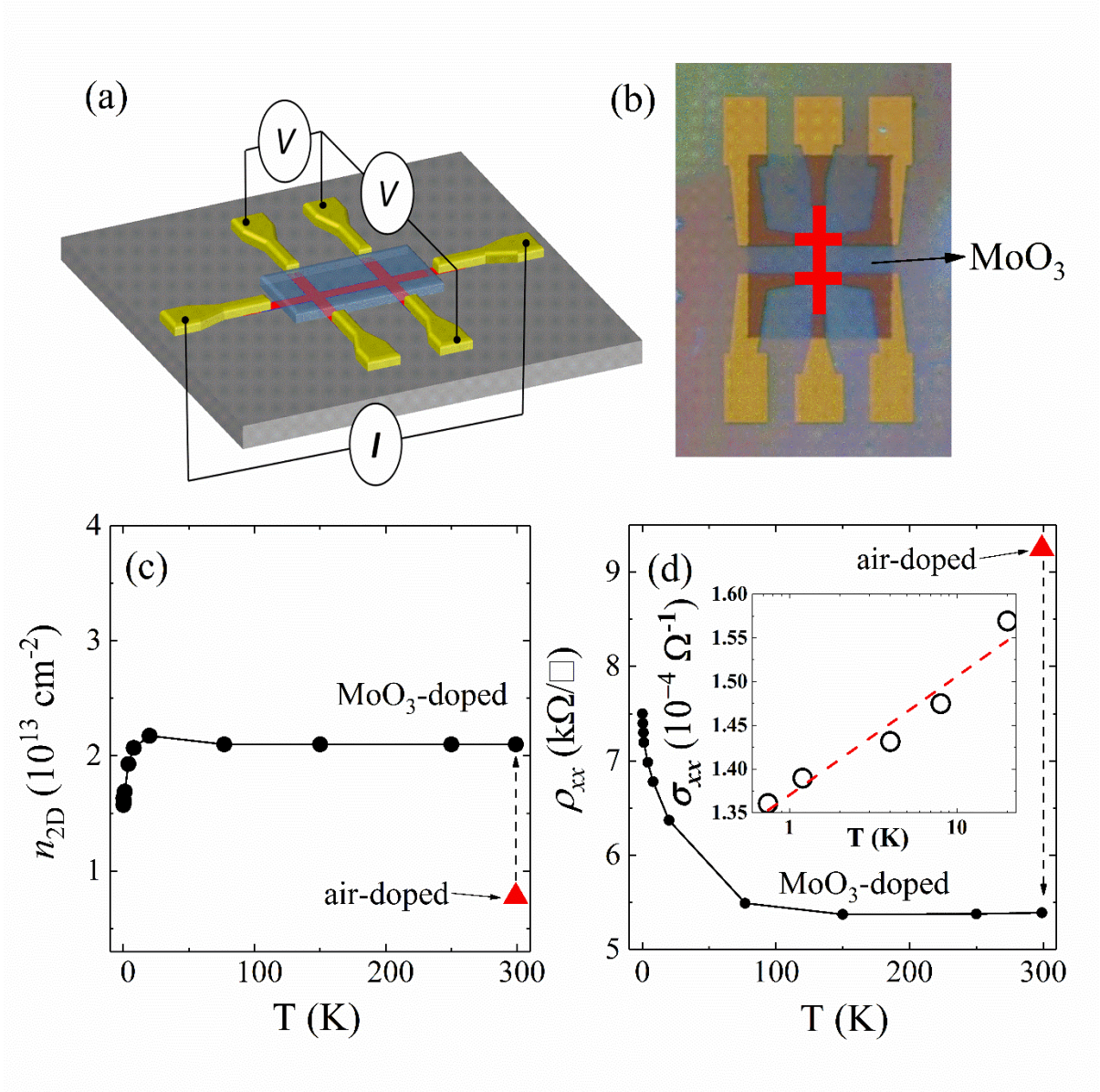


Figure 2. Variable-temperature transport characterisation for MoO_3 doped hall bar devices: (a) A schematic representation showing the electrical connections of the MoO_3 doped hall bar device. (b) A top-down optical image of the MoO_3 doped hall bar device, the red region represents the hall bar active region with hydrogen termination. (c) Hole density of hydrogen-terminated diamond as a function of temperature from 250 mK to 300 K. (d) Sheet resistivity of hydrogen-terminated diamond as a function of temperature from 250 mK to 300 K. Inset in (d) illustrates the linear relationship between the sheet conductivity and $\ln(T)$ from 250 mK to 20 K.

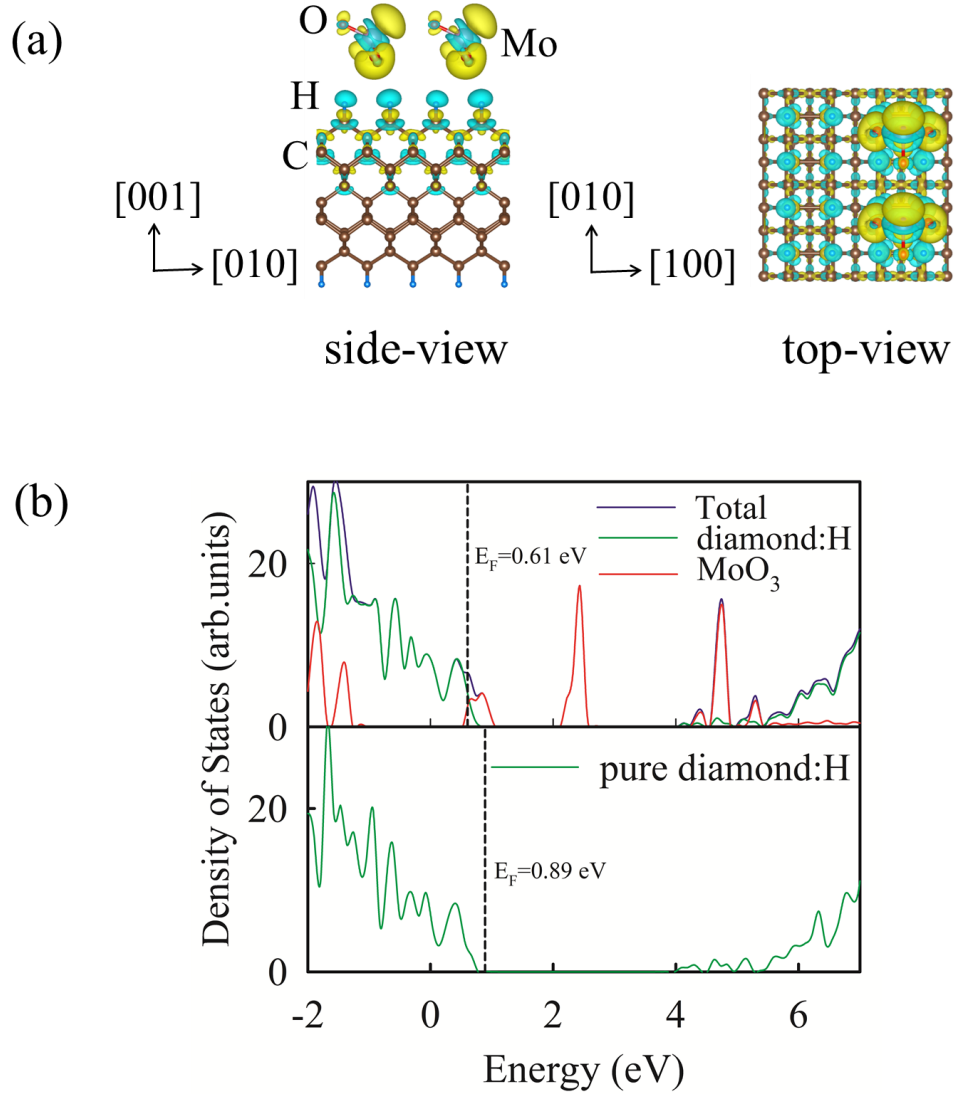


Figure 3. (a) Side and top view of charge density differences for the most preferable configuration of MoO₃-adsorbed hydrogen-terminated diamond surface. Yellow and blue regions represent electron and hole accumulations, respectively. (b) Density of states distribution of MoO₃-doped hydrogen-terminated diamond surface and the pristine hydrogen-terminated diamond surface. E_F denotes the Fermi level.